Korean J. Chem. Eng., 40(7), 1686-1698 (2023)
DOI: 10.1007/s11814-023-1379-1

pISSN: 0256-1115
eISSN: 1975-7220

Effect of manganese doping on the PbO_2 electrode for the enhanced electrochemical oxidation of anthracene: Optimization and mechanism

Jinjin Zhou*,, Xiuzhen Hao*, Longgang Chu*,**, and Long Cang*,†**

*Key Laboratory of Soil Environment and Pollution Remediation, Institute of Soil Science, Chinese Academy of Sciences, Nanjing 210008, China
**University of Chinese Academy of Sciences, Beijing 100049, China
(*Received 11 July 2022 • Revised 24 November 2022 • Accepted 16 December 2022*)

Abstract−Organic pollutant removal can be realized via electrochemical degradation, and anodic oxidation plays an important role in the degradation process. However, the degradation process is hindered by low removal efficiency and reusability. In this study, a PbO_2 electrode and a Mn-doped PbO_2 (Mn-PbO_2) electrode were prepared via electrodeposition. Different from the traditional method of increasing the oxygen evolution potential (OEP) of PbO_2 electrode, such as introducing Ce, Bi, and La in PbO_2 electrode, introducing Mn in PbO_2 electrode promoted the generation of strong oxidant MnO_4^- under electrolytic conditions to remove organic pollutants. The Mn-PbO_2 electrode was used for anthracene (ANT) degradation and the results showed that an ANT removal efficiency of 91.28% was achieved in 120 min under the most suitable operational variables, namely, a Na_2SO_4 concentration of 0.1 M, initial pH of 7, and current density of 20 mA/cm^2. In addition, the ANT degradation mechanism was analyzed. Given that the Mn-PbO_2 electrode exhibited better removal efficiency in the wide pH range and remarkable degradation efficiency compared with the PbO_2 electrode, the Mn-PbO_2 electrode has practical application prospects for organic pollutant degradation.

Keywords: Anodic Oxidation, Mn-PbO_2 Electrode, MnO_4^-, Anthracene, Degradation Mechanism

INTRODUCTION

The electrochemical advanced oxidation processes (EAOPs), a kind of AOPs, have attracted much attention because of strong oxidizing capacity, environmental friendliness, and good operability [1,2]. EAOPs depend on the formation of active species, including hydroxyl radicals ($^{\bullet}OH$), sulfate radical ($SO_4^{\bullet-}$), and oxidants, which have strong oxidizing capacity to decompose organic pollutants [3]. Among the EAOPs, anodic oxidation depends on reactive oxygen species (ROS), oxidants, and direct electron transfer (DET) process, and it is widely used for organic pollutant removal [4].

Regarding anodic oxidation, anode materials have great influence on the degradation process, and different anode materials have been investigated in previous studies, including dimensionally stable anodes SnO_2 [5], RuO_2-IrO_2 [6], PbO_2 [7,8], graphite [9], and boron-doped diamond (BDD) [10]. Among these electrodes, the PbO_2 electrode is a promising electrode owing to easy preparation, low cost, and high oxygen evolution potential (OEP) [11]. However, the PbO_2 electrode will slowly fail in the pollutant degradation process. Previous studies have found that improving the PbO_2 electrode by adopting Ti as the substrate [12,13] and Sb-doped SnO_2 (SnO_2-Sb) as the interlayer can effectively change the electrode stability and service life [14].

Much effort has been made to improve the OEP and specific surface area of the PbO_2 electrode [15]; for example, the electrode has been doped with transition metals and rare-earth metals elements, such as Cu [16], Bi [17], and Ce [18]. However, few researchers have investigated the modification of PbO_2 electrodes with Mn. Li et al. [19] declaring that a larger electrolyte resistance with a smaller charge transfer resistance of the Ti/SnO_2-Sb-Mn/PbO_2 electrode (Mn doping in the interlayer) led the decrease in electrical conductivity and increase in electron-capture capacity of MnO_x during phenol oxidation. Lin et al. [5] used three kinds of anodes (Ti/SnO_2-Sb, Ti/SnO_2-Sb/PbO_2, Ti/SnO_2-Sb/MnO_2) to degrade perfluorooctanoic acid (PFOA). The results indicated the degradation ratio of PFOA by Ti/SnO_2-Sb/MnO_2 was the lowest (only 31.7%), which indicated that the layer of MnO_2 on Ti/SnO_2-Sb electrode surface decreased the electron transfer ability. Lv et al. [20] studied the electrochemical performance improvement with Co and Mn doping in PbO_2 electrode (stainless steel sheet as substrate) by micro-area surface investigation. However the degradation ability of pollutants was not verified in practice. Thus, the modification effect of PbO_2 electrode with Mn was uncertain. Especially it is not clear how doping with Mn affects pollutant degradation and the quantitative and contribution analysis of ROS in the process of anodic oxidation of organic contaminant. Hence, it is vital to study the effect of Mn-doped PbO_2 electrodes on pollutant degradation and further analyze the process of pollutant degradation by the Mn-PbO_2 electrode.

Polycyclic aromatic hydrocarbons (PAHs), a priority organic pollutant, have been widely found in soil and sediment [21-23]. Some treatment technologies (leaching, thermal desorption, chemical oxidation, electrokinetic, microbial remediation, etc.) have been developed to remediate the PAHs contaminated soil and sediment. During leaching and electrokinetic remediation of PAHs contaminated soil

†To whom correspondence should be addressed.
E-mail: canglong@issas.ac.cn

with surfactants, the leaching solution and electrolyte containing PAHs need further treatment [24,25]. EAOPs is an effective treatment technology for the wastewater contained PAHs. In our study, Anthracene (ANT) was chosen as a model PAHs pollutant because of its wide distribution and persistency in the environment.

The purpose of this study is to explore the possibility of the electrochemical degradation of PAHs by Mn doping in the surface of PbO_2 electrode. In this work, an Mn-PbO_2 electrode was prepared via a combination of sol-gel and electrodeposition methods. The structure characterization, electrochemical measurement, and reusability of the Mn-PbO_2 electrode were conducted. The Mn-PbO_2 electrode was used as the anode to explore the most suitable electrolyte concentration, current density, and initial pH. And the contribution of anodic oxidation by ROS and oxidants and the DET process was investigated. Additionally, the main intermediates during the ANT degradation were identified, and a possible degradation mechanism of ANT was determined according to the intermediates.

MATERIALS AND METHODS

1. Chemicals and Solutions

Anthracene (99%), sodium sulfate (Na_2SO_4, 99%), Tween 80 (98%), stannic chlorid ($SnCl_4{\cdot}4H_2O$, 98%), antimony chloride ($SbCl_3$, 99%), potassium dichromate (K_2CrO_4, 99.8%), lead oxide (PbO, 99%), lead nitrate ($Pb(NO_3)_2$, 99%), sodium hydroxide (NaOH, 97%), sodium fluoride (NaF, 99%), manganous nitrate ($Mn(NO_3)_2$, 50%), terephthalic acid (TPA, 99%) and 2,5-dihydroxy terephthalic acid (98%) were obtained from China National Medicines Corporation Ltd. (Beijing, China). 5,5-Dimethyl-1-pyrroline N-oxide (DMPO) was purchased from J&K Scientific Ltd. (Shanghai, China). High-performance liquid chromatography (HPLC) grade methanol was obtained from Sigma-Aldrich (Saint Louis, MO, USA). Other chemicals and solvents used in this study were of analytical grade or HPLC grade.

2. Electrode Preparation

The Ti/SnO_2-Sb/PbO_2 electrodes (referred to as PbO_2 electrodes) were prepared as follows: First, the Ti substrate, which was rectangular (40 mm×20 mm×1 mm), was pretreated. It was polished with 600-, 800-, and 1,200-mesh sandpaper to obtain a flat surface. Afterward, it was ultrasonically cleaned in 20% acetone for 20 min, anhydrous ethanol for 20 min, and ultrapure water for 30 min and then etched in 10% oxalic solution at 85 °C for 2 h to obtain a rough surface. Second, the SnO_2-Sb layers were fabricated on the pretreated Ti substrate via the sol-gel method according to the study by Lin et al. [26]. The substrate was dipped in a solution of $SnCl_4{\cdot}4H_2O$: $SbCl_3$ (molar ratio=9 : 1) for 10 min, dried at 140 °C, and subjected to thermal decomposition at 500 °C. The sol-gel process was repeated 15 times, whereby in the last run, the thermal decomposition lasted for 2 h to obtain the SnO_2-Sb layer. Then, α-PbO_2 layers were fabricated on the SnO_2-Sb layers via electrodeposition in alkaline electrolyte containing 140 g/L NaOH, 22.32 g/L PbO, and 10 g/L K_2CrO_4 at 40 °C and a constant current density of 2 mA/cm^2 for 60 min. Finally, β-PbO_2 layers were also generated via electrodeposition in an acidic electrolyte containing 0.5 M $Pb(NO_3)_2$, 0.1 M HNO_3, and 0.04 M NaF at 60 °C and a constant current density of 20 mA/cm^2 for 60 min to obtain the PbO_2 electrode.

For the Mn-PbO_2 electrodes (Ti/SnO_2-Sb/Mn-PbO_2), their preparation method was similar to the above-described electrodeposition method: except for the different electrolyte components in the last step: the Mn-PbO_2 electrode was prepared by the addition of $Mn(NO_3)_2$ to an acidic electrolyte containing 0.5 M $Pb(NO_3)_2$, 0.1 M HNO_3, and 0.04 M NaF. According to the preliminary experiment, we determined that the optimal concentration of $Mn(NO_3)_2$ was 3 mM (see Fig. S1).

3. Characterization and Electrochemical Performances

The surface morphology and composition of the as-prepared electrodes were analyzed via scanning electron microscopy (SEM: JSM-7800F, Japan) coupled with energy-dispersive spectroscopy (EDS: Zeiss Sigma 300, Germany). The crystal structure and the surface chemical states of the as-prepared electrodes were investigated via X-ray diffraction (XRD, Brooke D8 Advance, Germany) and X-ray photoelectron spectroscopy (XPS, Thermo Scientific K-Alpha, USA), respectively.

Electrochemical performance tests, namely linear sweep voltammetry (LSV) and cyclic voltammetry (CV), were performed on the as-prepared electrodes using an electrochemical workstation (RST 5000, Zhengzhou, China) with the conventional three-electrode system Tan et al. [27]. The as-prepared electrodes were used as the working electrodes, while a platinum wire and a Ag/AgCl electrode served as the counter electrode and reference electrode, respectively. The voltammetric charge (q*, C) of electrodes was calculated by the integral area of CV curves as follows:

$$q^* = \int I \cdot \varphi \cdot v^{-1} \, d\varphi$$

where I is the current (A), φ is potential difference (V), and v is scan rate (mV/s).

4. Electrocatalytic Oxidation of ANT

Anthracene was selected as the model pollutant, and its concentration was constant at 1 mg/L. Tween 80 (5 g/L) was added to the electrolytic cell to dissolve ANT. Na_2SO_4 was used as the supporting electrolyte throughout the experiment [16]. The ANT degradation experiments were performed in a 200 ml cylindrical electrolytic cell with an effective electrolyte volume of 150 ml. The as-prepared PbO_2 electrodes and Mn-PbO_2 electrodes were used as the anode, and Ti sheets with the same area (40 mm×20 mm) were used as the cathode. The distance between the anode and cathode was constant (30 mm), and the current was controlled by a DC power supply (DP 832, RIGOL, China). The as-prepared electrodes were used to decompose ANT to evaluate the effect of the main operational variables on the ANT removal efficiency and the pseudo-first-order kinetic reaction rate constant (k). The concept of ANT removal efficiency was defined by the ratio of the removed ANT concentration and the original ANT concentration. The main operational variables were concentration of supporting electrolyte (0.05, 0.1, 0.15, 0.2 M Na_2SO_4); current density (10, 20, 30, 40 mA/cm^2); and initial pH of electrolyte (3, 5, 7, 9, 11), which was adjusted by H_2SO_4 or NaOH solution. Each experiment was repeated three times, each experiment lasting 120 min. Solution samples were taken every 30 min, and an equivalent amount of methanol was added to analyze the removal efficiency.

5. Analysis Methods

The ANT concentration during the electrocatalytic oxidation was

quantified via high-performance liquid chromatography (Shimadzu, LC-10A, Japan) coupled with UV detection, with methanol and ultrapure water as the mobile phase. The intermediates of ANT after 60 min and 120 min of electrocatalytic oxidation in 0.1 M Na_2SO_4 solution containing 1 mg/L ANT at a constant current density of 20 mA/cm^2 were determined via gas chromatography-mass spectrometry (GC-MS: QP2010 Ultra, Shimadzu, Japan) and ultra-performance liquid chromatography-quadrupole-time of flight-mass spectrometry (LC-TOF-MS: X5000R, AB, America). Specific operation details can be found in Text S1 and Text S2.

Electron paramagnetic resonance (EPR) spectra were obtained by a Bruker E500-9.5/12 E5010003 spectrometer (Bruker Co., Germany). DMPO was used as a trapping agent and •OH could be detected by determination of the signal peaks of DMPO-OH. More operation details can be found in Text S3. The •OH radicals formed from the anode and their concentrations were determined using

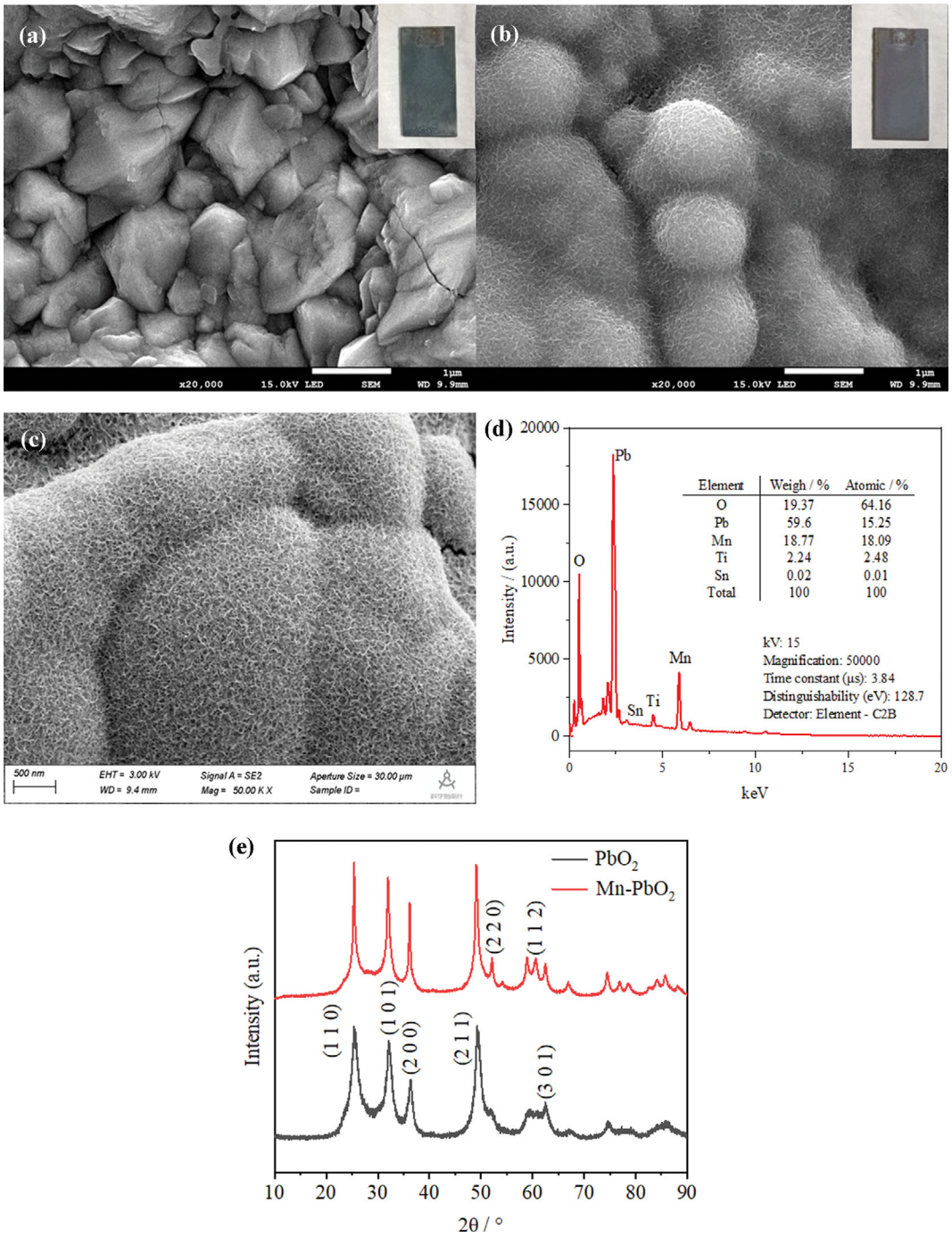

Fig. 1. SEM images of (a) PbO_2, (b) Mn-PbO_2, (c) enlarged figure of Mn-PbO_2 electrodes, (d) EDS spectrum and elemental mapping analysis of Mn-PbO_2 electrode and (e) XRD patterns of the PbO_2 and Mn-PbO_2 electrodes (the image in the upper right corner was the photograph of PbO_2 and Mn-PbO_2 electrode in Fig. 1(a) and (b)).

TPA as the scavenger according to Tang et al. [28], and the operation details can be found in Text S4.

When the Mn-PbO_2 electrode was used as the anode in 0.1 M Na_2SO_4 solution at a constant current density of 20 mA/cm^2 in an electrolytic cell, the purplish-red oxidant MnO_4^- was observed in the electrolytic system. Solution samples taken from the electrolytic cell at 0, 5, 10, 15, 20, 30, 60, 90, and 120 min were analyzed via UV-vis spectrophotometry (UV-2700, Shimazu, Japan) at 250-750 nm and 525 nm, and the same anode was used three times.

Radical inhibition experiments were performed to explore the roles of ROS, oxidants, and the DET process during ANT degradation. Ethanol was selected to scavenge $^{\bullet}OH$ and $SO_4^{\bullet-}$ according to Chen et al. [29]. The effects of different concentrations of ethanol (1 M and 2 M) on the ANT removal were investigated.

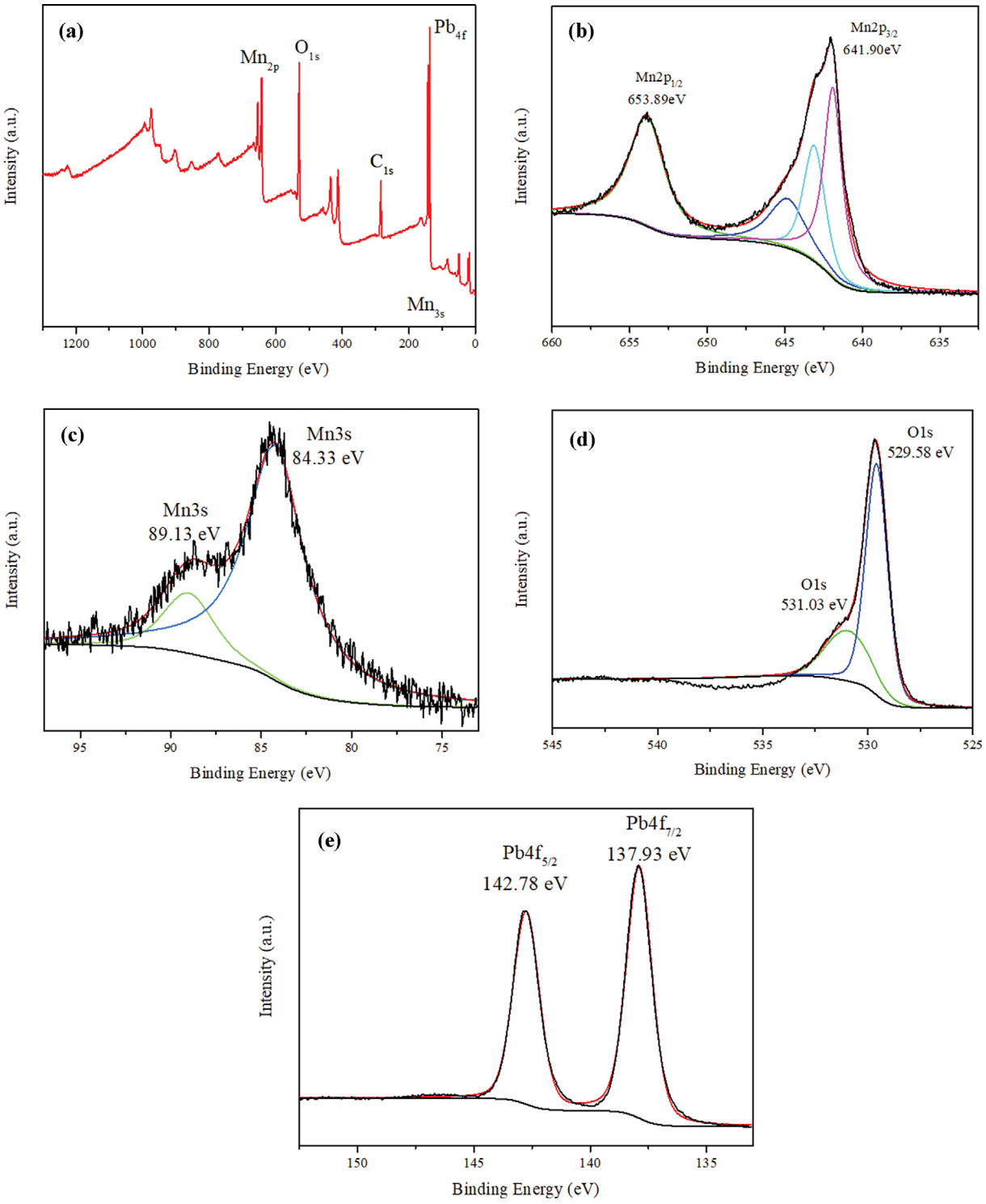

Fig. 2. XPS spectrum of Mn-PbO_2 electrode: (a) total spectrum, (b) Mn 2p spectrum, (c) Mn 3s spectrum, (d) O 1s spectrum, (e) Pb 4f spectrum.

The reusability of the as-prepared electrodes was determined based on the ANT removal efficiency in 0.1 M Na_2SO_4 solution at a constant current density of 20 mA/cm^2 and an electrolysis time of 120 min; in the test, the same anode was used ten times.

The metals leaching concentration including Pb and Sb was determined by flame atomic absorption spectrophotometer (FAAS, Z-2000, Hitachi, Japan). Each experiment was repeated three times and the detection limit is 0.1 mg/L for Pb and Sb. The PbO_2 and Mn-PbO_2 electrodes were used as the anode respectively in ANT-free 0.1 M Na_2SO_4 solution at a constant current density of 20 mA/cm^2 in an electrolytic cell and solution samples were taken from the electrolytic cell at 0, 30, 60, 90, and 120 min.

RESULTS AND DISCUSSION

1. Characterization of As-prepared Electrodes

As is well known, the structure and particle size have great influence on the electrochemical properties of electrodes [30]. The SEM images of PbO_2, and Mn-PbO_2 and the enlarged image of Mn-PbO_2 electrodes are displayed in Fig. 1(a)-(c). As shown in Fig. 1(a), the dense α-PbO_2 particles formed in alkaline electrolyte may be conducive to the formation of β-PbO_2 particles and improve the β-PbO_2 electrode electrochemical stability owing to the crystal structure characteristics [31]. The dense α-PbO_2 particles can effectively prevent the electrolyte from entering into the Ti substrate and destroying the active layer, thus increasing the electrode service life. From Fig. 1(b), many pyramid crystal-shaped particles occurred on the PbO_2 electrode surface [32]. Introduction of Mn into PbO_2 changed the crystal structure of the electrode (Fig. 1(c)), and the Mn formed many subgrains on the electrode surface [33]. Therefore, the introduction of Mn in PbO_2 increased the number of active sites of the electrode. In addition, Fig. 1(d) present the EDS spectrum and elemental mapping analysis results. The surface elements of the Mn-PbO_2 electrodes were O, Pb, Mn, Ti and Sn with atomic ratios of 64.16%, 15.25%, 18.09%, 2.48% and 0.01% respectively. The reason why Sb element was not detected by EDS may be that the content of Sb in the Mn-PbO_2 electrode was so low that its concentration was below the detection limit.

Fig. 1(e) presents the XRD patterns of the PbO_2 and Mn-PbO_2 electrodes, respectively. The diffraction peaks indexed to PbO_2 at 25.37°, 31.98°, 36.18°, 49.05°, and 62.45° are assigned to the (1 1 0), (1 0 1), (2 0 0), (2 1 1), and (3 0 1) planes of PbO_2, respectively, which is consistent with the standard data of the JCPDS card (number: 76-0564). For the Mn-PbO_2 electrode, the diffraction peaks indexed to Mn-PbO_2 at 25.37°, 31.98°, 36.18°, 49.05°, 52.10°, 60.71°, and 62.45° are assigned to the (1 1 0), (1 0 1), (2 0 0), (2 1 1), (2 2 0), (1 1 2) and (3 0 1) planes of PbO_2, respectively, which is also consistent with the JCPDS card (number: 76-0564) [34]. Furthermore, the XRD pattern of PbO_2 featured no diffraction peak of MnO_2 because of the low dopant levels in PbO_2. It is difficult to show corresponding diffraction peaks for the doping of a small amount of transition metals, which is consistent with previous study [35].

Furthermore, XPS was adopted to obtain the surface chemical state of the Mn-PbO_2 electrode, and the results are shown in Fig. 2. Fig. 2(a) presents the XPS total spectrum of the Mn-PbO_2 electrode. Fig. 2(b) displays the detailed scan spectra of Mn 2p. The spectra display two major peaks, at 641.90 eV and 653.89 eV, corresponding to Mn $2p_{3/2}$ and Mn $2p_{1/2}$, respectively. The result indicates that Mn existed as Mn (IV). Moreover, the Mn 3s spectrum (Fig. 2(c)) featured two peaks, at 84.33 eV and 89.13 eV, and the binding energy difference between 84.33 eV and 89.13 eV was 4.8 eV. These findings show that MnO_2 was formed in the electrodes [36]. The O 1s spectrum (Fig. 2(d)) featured two major peaks, at 529.58 eV and 531.03 eV, verifying the formation of PbO_2 on the electrodes and the adsorption of a small amount of water on the surface. The detailed scan spectra of Pb 4f (Fig. 2(e)) featured two major peaks, at 137.93 eV and 142.78 eV, corresponding to Pb $4f_{7/2}$ and Pb $4f_{5/2}$, respectively. The difference of almost 4.85 eV between Pb $4f_{5/2}$ and Pb $4f_{7/2}$ was proposed by Xie et al. [8], suggesting that PbO_2 was formed on the electrodes.

2. Electrochemical Performance of As-prepared Electrodes

LSV curves were used to evaluate the O_2-production ability of the anode through OEP. Lower OEP results in higher energy consumption in pollutant degradation, and higher OEP can effectively improve the pollutant degradation efficiency by reducing side reac-

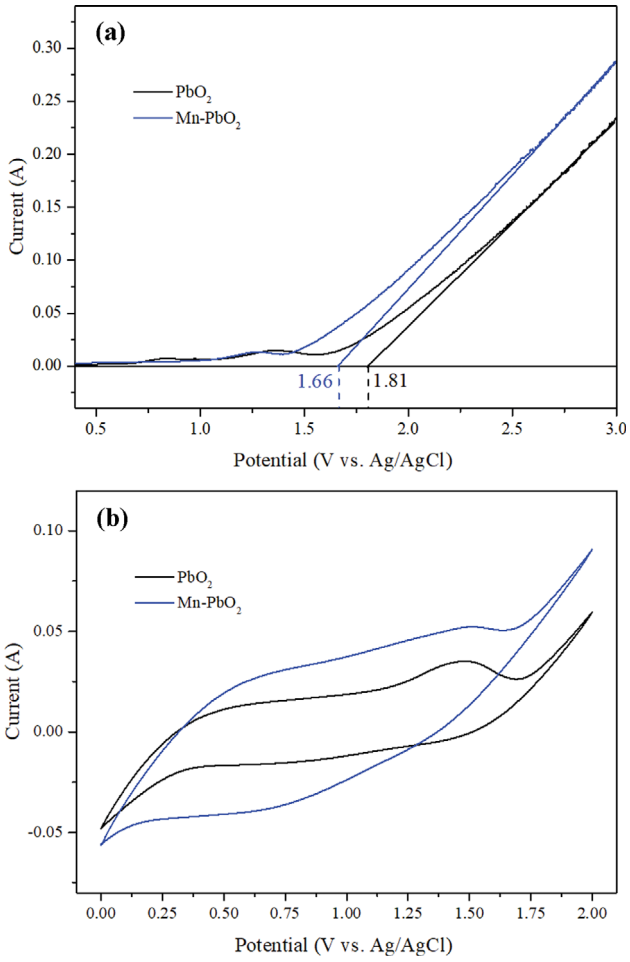

Fig. 3. (a) LSV curves of the PbO_2 and Mn-PbO_2 electrodes in 0.1 M Na_2SO_4 solution with initial pH of 7 at a scan rate of 1 mV/s and (b) CV curves of the PbO_2 and Mn-PbO_2 electrodes in 0.1 M Na_2SO_4 solution with initial pH of 7 at a scan rate of 20 mV/s.

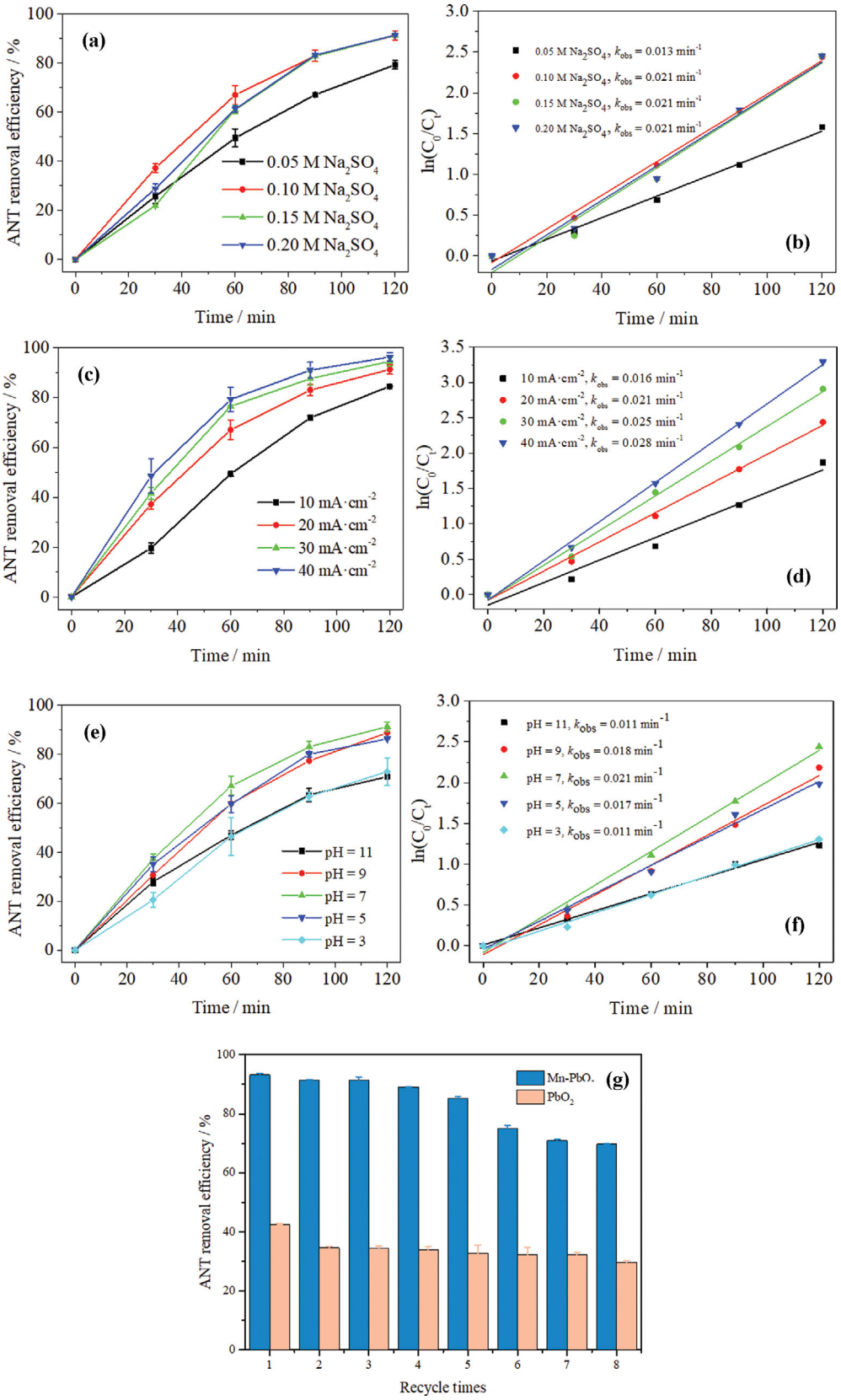

Fig. 4. Effect of Na_2SO_4 concentration (initial pH: 7±0.3, 20 mA/cm^2), current density (initial pH: 7±0.3, 0.1 M Na_2SO_4) and initial pH (current density: 20 mA/cm^2, 0.1 M Na_2SO_4) on ((a), (c), (e)) the ANT removal efficiency and ((b), (d), (f)) the corresponding kinetics analysis in 1 mg/L ANT solution by Mn-PbO_2 electrode; (g) effect of recycle times on degradation of ANT by the PbO_2 and Mn-PbO_2 electrodes in 0.1 M Na_2SO_4 solution (current density: 20 mA/cm^2; initial pH: 7±0.3; initial ANT concentration: 1 mg/L).

tion of oxygen evolution [37]. Fig. 3(a) shows the LSV curves of the PbO_2 and Mn-PbO_2 electrodes in 0.1 M Na_2SO_4 solution with an initial pH of 7 at a scan rate of 1 mV/s. The OEP of the Mn-PbO_2 electrode was observed to be ~1.66 V (vs. Ag/AgCl), which is lower than the OEP of the PbO_2 electrode (~1.81 V, vs. Ag/AgCl). The Mn-doped PbO_2 reduced the OEP and influenced the electrocatalytic performance of the electrode in ways different from the Bi-doped PbO_2 electrode and Ce-doped PbO_2 electrode [17,35].

CV curves were used to measure electrochemically active surface sites and test the electrochemical activity of the electrodes. Fig. 3(b) displays the CV curves of the PbO_2 and Mn-PbO_2 electrodes in 0.1 M Na_2SO_4 solution with an initial pH of 7 under a scan rate of 20 mV/s. For the PbO_2 electrode, in the positive scan, the oxidation peaks were 1.33 V (vs. Ag/AgCl), which corresponds to the transformation of $PbSO_4$/PbO_2, and in the reversed scan, the reduction peaks were 0.876 V (vs. Ag/AgCl), which corresponds to the transformation of PbO_2/$PbSO_4$ [38,39]. Fig. 3(b) illustrates that for the Mn-PbO_2 electrode, in 0.1 M Na_2SO_4 solution, there were no significant oxidation peaks at 1.33 V (vs. Ag/AgCl) and reduction peaks at 0.876 V (vs. Ag/AgCl) in the CV curves and that the Mn-PbO_2 electrode was in a stable state.

Moreover, the voltammetric charge (q*) was used to determine the electrochemically active surface sites and evaluate the catalytic performance [40]. Fig. 3(b) demonstrates that the q* of the Mn-PbO_2 electrode (q*=3.7949 C) was higher than that of the PbO_2 electrode (q*=2.1003 C). By comparison, the results show that the introduction of MnO_2 into PbO_2 can improve the electrode stability and increase electrochemically active surface area in pollutant degradation [41].

3. Optimization of Electrocatalytic Oxidation Condition of ANT

3-1. Effect of Na_2SO_4 Concentration

Investigating the effect of electrolyte concentration is important, as the electrolyte can improve the solution conductivity and provide strong oxidants and free radicals, such as $S_2O_8^{2-}$ and $SO_4^{\bullet-}$ [42]. As shown in Fig. 4(a), the ANT removal efficiencies in 0.05, 0.1, 0.15, and 0.2 M Na_2SO_4 solutions were 79.37%, 91.28%, 91.39%, and 91.38%, respectively. Moreover, Fig. 4(b) shows that the ANT removal efficiency under different electrolyte concentrations conformed to a pseudo-first-order kinetics model (R^2>0.97), and the maximum k value (k=0.021 min^{-1}) corresponded to 0.1, 0.15 and 0.2 M Na_2SO_4 solutions.

The results demonstrate that when the electrolyte concentration reached a certain value, the ANT removal efficiency did not increase with the electrolyte concentration. One possible explanation for this occurrence is that the redundant SO_4^{2-} migrated to the anode and became adsorbed on the anode, preventing ANT from contacting the anode, as reported by Yu et al. [43]. As a result, considering raw material cost, the electrolyte concentration of 0.1 M Na_2SO_4 was selected as the most suitable operational variable for the following experiments.

3-2. Effect of Current Density

In an electrochemical system, the current density has an important effect on the organic pollutant degradation process, as it can influence the electron transfer rate and $^{\bullet}OH$ radical generation rate [18]. As presented in Fig. 4(c), the ANT removal efficiencies at 10, 20, 30, and 40 mA/cm^2 were 84.51%, 91.28%, 94.53%, and 96.28%, respectively. In addition, Fig. 4(d) illustrates that the ANT removal efficiency under different current densities followed a pseudo-first-order kinetics model (R^2>0.97), and the maximum k value (k= 0.028 min^{-1}) corresponded to the current density of 40 mA/cm^2.

The ANT removal efficiency significantly increased with the increase of current density (Fig. 4(c)), because the $^{\bullet}OH$ formation increased with the current density [44], which can promote the ANT degradation process. However, under a high current density, side reactions were promoted, including hydrogen evolution and oxygen evolution [45,46]. In addition, the ANT removal efficiency at 40 mA/cm^2 was not significantly higher than that at 20 mA/cm^2; therefore, considering cost and the ANT removal efficiency, the current density of 20 mA/cm^2 was chosen as the most suitable operational variable in the rest experiments.

3-3. Effect of Initial pH

Investigating the effect of the initial pH of Na_2SO_4 solution is important because the initial pH of the solution is not constant in many practical applications [47]. The Mn-PbO_2 electrode was applied to decompose ANT in solutions with initial pH values of 3, 5, 7, 9, and 11. The ANT removal efficiencies in 0.1 M Na_2SO_4 solutions with initial pH values of 3, 5, 7, 9, and 11 were 72.88%, 86.23%, 91.28%, 88.73%, and 70.84%, respectively (Fig. 4(e)). In addition, the ANT removal efficiencies under different initial pH conditions followed a pseudo-first-order kinetics model (R^2>0.98), and the k value (0.021 min^{-1}) was maximum at an initial pH of 7 (Fig. 4(f)).

Under strongly acidic conditions, the organic pollutant removal efficiency may be limited by the oxidants or other factors. Other studies have observed that $SO_4^{\bullet-}$ in Na_2SO_4 solution showed poor oxidizing ability under acidic conditions [42,48,49]. Additionally, electrode passivation occurred in the highly alkaline environment, which inhibited the generation of $^{\bullet}OH$ [50] and reduced the ANT degradation rate in the Na_2SO_4 solution. Overall, the ANT removal efficiency was always maintained above 70% under a wide pH range, and pH 7 was chosen as the most suitable operational variable.

3-4. Reusability and Safety Evaluation of Mn-PbO_2 Electrodes

The reusability of electrode was the key factor for its industrial application, which affected the cost and efficiency of pollutant treatment. Fig. 4(g) shows the effects of the PbO_2 and Mn-PbO_2 electrodes on ANT degradation in 0.1 M Na_2SO_4 solution containing 1 mg/L ANT at eight recycle times (120 min every time). The ANT removal efficiencies of the PbO_2 electrode after the 1st and 8th degradation cycles were 42.5% and 29.7%, respectively, whereas those of the Mn-PbO_2 electrode were 93.3% to 70.0%, respectively. The result demonstrated that the Mn-PbO_2 electrode had excellent recyclability and more practical application potential than the PbO_2 electrode.

The main drawback of the PbO_2 electrodes as anode is the possible leaching of metal ions during the electrochemical oxidation. Therefore, the safety of as-prepared electrodes was evaluated by FAAS under electrocatalytic conditions. As shown in Table S2, when the PbO_2 and Mn-PbO_2 electrodes were used as anode, Pb and Sb ions were not detected by FAAS. The concentration of metals was below 0.1 mg/L. Therefore, there was no secondary pollution of metals including Pb and Sb. These results were similar to the reports of Labiadh et al. [7] and Wei et al. [47]. In these studies, the lead

ions were not detected in solution by AAS during the electrochemical degradation of pollutants by Ti/PbO_2 and Ti/TiO_2-NT_S/PbO_2 electrodes. However, some certain environments (higher pH and chloride concentration) could enhance the corrosion and dissolution of the PbO_2 electrode [51,52]. Therefore, to avoid leaching of metal ions and protect water quality, higher pH and chloride concentration environment should be avoided in practical applications for organic pollutant degradation.

4. Degradation Mechanism of ANT

4-1. Analysis of ANT Intermediates and Possible Degradation Pathway

The ANT concentration was quantified via high-performance liquid chromatography, but the ANT intermediates were analyzed via GC-MS and LC-TOF-MS. Through qualitative analysis of the intermediates, a possible degradation pathway of ANT can be obtained. As presented in Table S1, ANT (A1) and ATQ (A2) were detected via GC-MS, and their retention times were 8.485 min and 9.945 min, respectively, which correspond to Fig. 5(a) and Fig. 5(b), respectively. In addition, 1-hydroxyATQ (1-hATQ, A3), 1,5-dihydroxyATQ (1,5-dhATQ, A4), 1,2,4-trihydroxyATQ (1,2,4-thATQ, A5), and 1,9,10-trihydroxyANT (1,9,10-thANT, A6) were detected via LC-TOF-MS (Fig. S2). Hence, from Fig. 5(c), one of the possible degradation pathways is that ANT was oxidized to A6 during oxidation. Another possible degradation pathway is that

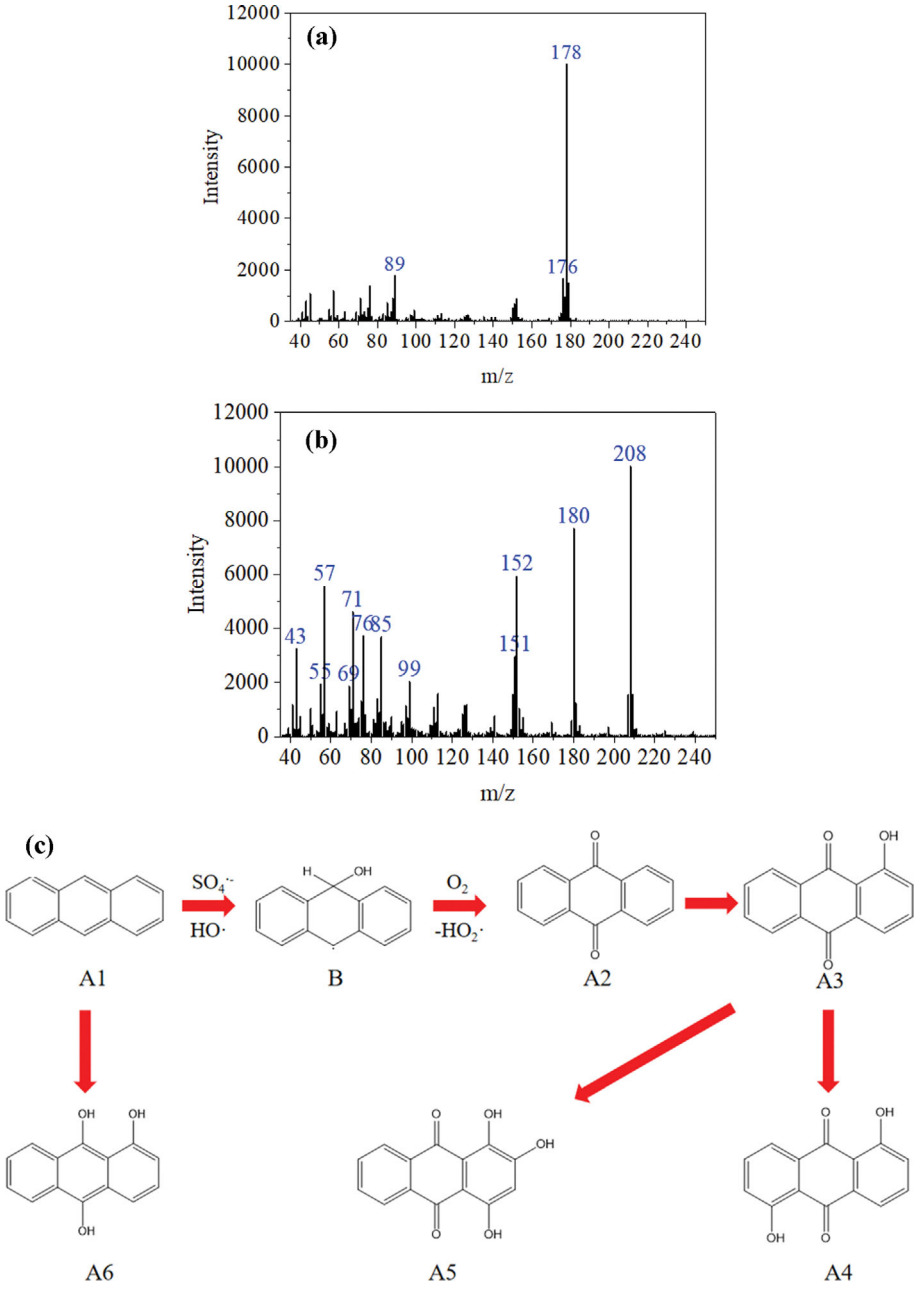

Fig. 5. MS spectrum of (a) ANT, (b) ATQ in GC-MS and (c) possible degradation pathway of ANT under electrocatalytic conditions (A1: ANT; A2: anthraquinone (ATQ); A3: 1-hydroxy ATQ; A4: 1,5-dihydroxy ATQ; A5: 1,2,4-trihydroxy ATQ; A6: 1,9,10-trihydroxy ANT).

ANT was converted into hydroxyl radical product B, which agrees with a previous study [53]. The hydroxyl radical product B was not stable and was easily converted to ATQ, which acted as the main degradation product of ANT [54]. Moreover, ATQ was oxidized to A3, A4, and A5 by oxidants and reaction with radical in sequence [55]. The ATQ products with hydroxyl groups may be transformed to other intermediates, but their concentrations were below the detection limit.

We used the ECOSAR v1.11 (https://www.epa.gov) to analyze the toxicity of the intermediates and ANT (A1). As shown in Table S3, we found that for fish and green algae, except for product A4, the acute toxicity of other intermediates was lower than that of ANT (LC_{50}/EC_{50} (ANT)<LC_{50}/EC_{50} (A2, A3, A5 and A6)). In addition, the acute toxicity of ANT intermediates was lower than that of ANT (LC_{50}/EC_{50} (ANT)<LC_{50}/EC_{50} (A2, A3, A4, A5 and A6)) for daphnia. Therefore, we suggest that the removal of ANT with the Mn-PbO_2 electrode is a process of acute toxicity reduction.

4-2. Analysis of ·OH Radicals

Generally, the ANT degradation process was mainly due to ROS such as ·OH and $SO_4^{\cdot-}$ radicals, oxidants such as MnO_4^-, and DET (Eq. (1), Eq. (2), and Eq. (3)) [42,56]. Hence, investigating the ANT degradation process is important.

$$PbO_2\ (H_2O) \rightarrow PbO_2\ (^{\cdot}OH) + H^+ + e^- \quad (1)$$

$$PbO_2\ (MnO_2) + 2H_2O \rightarrow PbO_2 + MnO_4^- + 4H^+ + 3e^- \quad (2)$$

$$ANT\ (DET) \rightarrow Intermediates \quad (3)$$

As shown in Fig. 6(a), there was no obvious peak in 0.1 M Na_2SO_4 as electrolyte in control treatment (without any electrode) in EPR spectrogram. The peak intensity ratio was 1 : 2 : 2 : 1 and ·OH (◆) can be observed by using BDD (40 mm×20 mm×1 mm) as anode, which agrees with that of DMPO-OH adducts [57]. When the PbO_2 and Mn-PbO_2 electrodes were used as anode, there was no peak of DMPO-OH in EPR spectra, and the reason might be the low ·OH concentration. Therefore, it was important to analyze the ·OH concentration and the results were as follows.

The generation of ·OH radicals affected the pollutant degradation. and the ·OH radical generation capability of the as-prepared electrodes was determined in 0.1 M Na_2SO_4 solution at a constant current density of 20 mA/cm^2 and an initial pH of 7 (Fig. 6(b)). The ·OH concentration of the PbO_2 and the Mn-PbO_2 electrodes was much lower than that of BDD electrode (4.03 μM). The results were consistent with the EPR spectra, because the low ·OH concentration made it difficult to generate signal peaks of DMPO-OH adducts. The ·OH concentration of the PbO_2 electrode was 1.34 μM, and the ·OH concentration of the Mn-PbO_2 electrode was only 0.70 μM. The results demonstrate that the ·OH radicals were continuously formed on the anode according to Eq. (1) [58]. However, the introduction of MnO_2 in PbO_2 reduced the ·OH radical generation capability. The results were consistent with the OEP results in terms of LSV curves, because the higher OEP of the PbO_2 electrode can reduce the side reaction of oxygen evolution to increase the ·OH radical generation capability [59]. Hence, the Mn-PbO_2 electrodes may not improve the removal efficiency of ANT by improving the ·OH concentration.

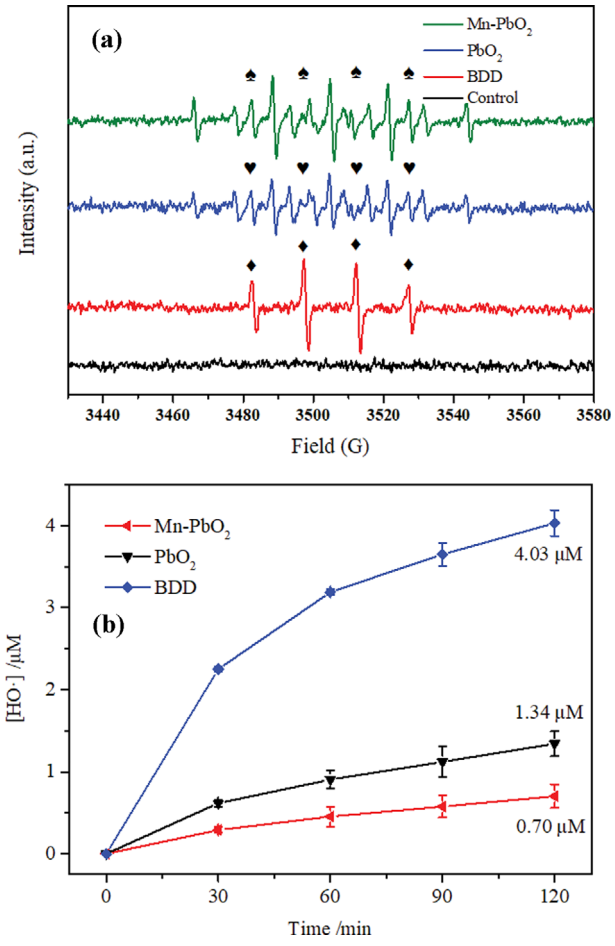

Fig. 6. (a) EPR spectra after 5 min in 0.1 M Na_2SO_4 electrolyte without any electrode (control) and with BDD, PbO_2 and Mn-PbO_2 electrode (current density: 40 mA/cm^2, initial pH: 7± 0.3) and (b) The ·OH concentration with the PbO_2, Mn-PbO_2, and BDD electrodes at different times in 0.1 M Na_2SO_4 solution (current density: 20 mA/cm^2, initial pH: 7±0.3).

4-3. Oxidant Analysis and Estimation of the Oxidant Contribution

The generation of oxidants on anode materials such as $S_2O_8^{2-}$ and ClO^- plays an important role in organic pollutant degradation [12,60]. In anodes such as BDD and PbO_2 electrodes, $S_2O_8^{2-}$ was produced by SO_4^{2-} in Na_2SO_4 solution [61]. Different from BDD and PbO_2 electrodes, MnO_4^- was produced on the Mn-PbO_2 electrode in the Na_2SO_4 electrolyte over time because of the introduction of MnO_2 into PbO_2 particles, as shown in Eq. (4). Fig. 7(a) presents the absorption intensities of the electrolyte in the 250-750 nm wavelength region and the MnO_4^- concentrations at different times in 0.1 M Na_2SO_4 solution with the Mn-PbO_2 electrode as the anode. The absorption intensity at 525 nm wavelength indexed to MnO_4^- was the maximum at each time point and gradually increased with electrolysis time from 0 min to 120 min. As shown in Fig. 7(b), the MnO_4^- concentration increased from 0 to 56.2 μM with electrolysis time from 0 min to 120 min. The results demonstrate that the Mn-PbO_2 electrode could produce MnO_4^- and the MnO_4^- concentration increased with electrolysis time.

From the above, for the Mn-PbO_2 electrode, it is important to

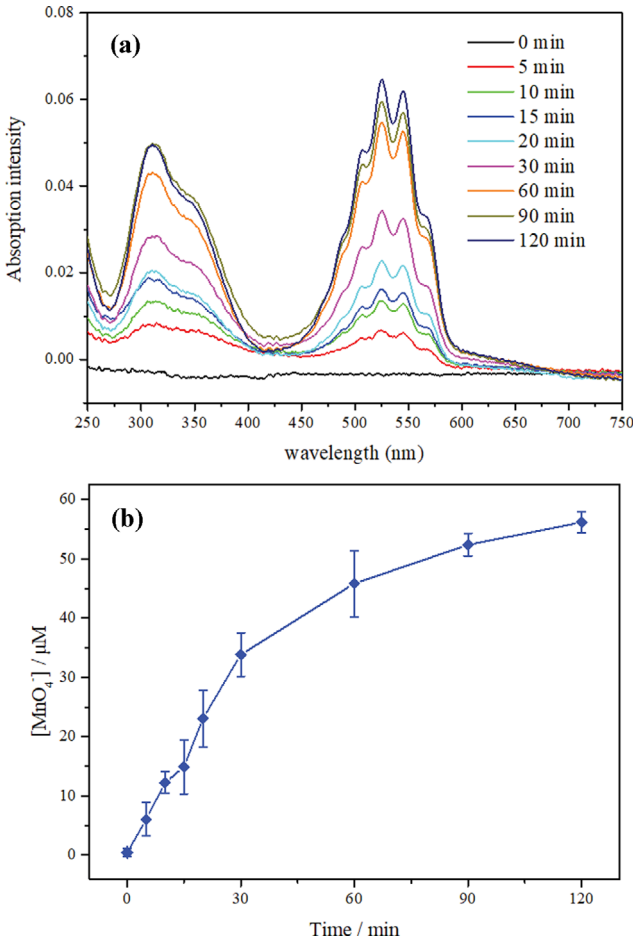

Fig. 7. (a) The absorption intensity of the electrolytes at different times in the range of 250-750 nm wavelength and (b) the concentration of MnO_4^- (current density: 20 mA/cm^2; initial pH: 7±0.3).

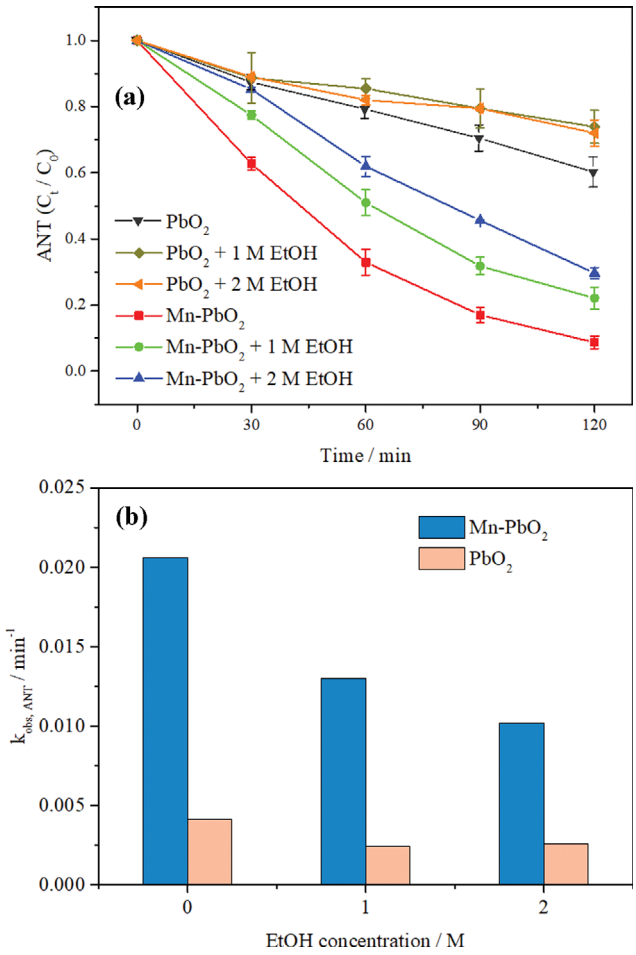

Fig. 8. (a) The removal efficiency of ANT and (b) the corresponding observed reaction rate (k_{obs}, ANT) in presence of 0-2 M EtOH (ethanol) with the PbO_2 and Mn-PbO_2 electrodes in 0.1 M Na_2SO_4 solution (current density: 20 mA/cm^2; initial pH: 7±0.3; initial ANT concentration: 1 mg/L).

estimate the oxidant contribution for degradation. Ethanol was selected to scavenge $^{\bullet}OH$ and $SO_4^{\bullet-}$ according to Chen et al. [29]. The ANT removal efficiency in Na_2SO_4 solution containing 1 mg/L ANT in the presence of 0-2 M EtOH with the PbO_2 and Mn-PbO_2 electrodes was investigated. As illustrated in Fig. 8(b), the inhibition effect of 1 M ethanol on the ANT removal efficiency (k=0.0024 min^{-1}) was close to that of 2 M ethanol (k=0.0026 min^{-1}) for the PbO_2 electrode. The results illustrate that 2 M ethanol could effectively quench ROS in the solution. For the Mn-PbO_2 electrode, the inhibition effect of 2 M ethanol on the ANT removal efficiency (k=0.0102 min^{-1}) was slightly higher than that of 1 M ethanol (k=0.0133 min^{-1}). The result indicates that 2 M ethanol could completely quench ROS. When the ROS was inhibited by ethanol, the ANT removal efficiency in the presence of MnO_4^- and DET reached 70.36% (Fig. 8(a)); thus, the combination of MnO_4^- and the DET process played a major role in improving the ANT removal efficiency rather than ROS.

5. Comparison of other Electrodes

To evaluate the practical application of the Mn-PbO_2 electrode in degrading organic pollutants, several common electrodes include BDD, Ru-IrO_2, Ru-SnO_2 and Pt through literature (Table 1). The Ru-IrO_2 electrode is often used in chloro-alkaline industry and degradation of organic pollutants such as dye (e.g. methylene blue) and industrial intermediates (e.g. aniline) because of its high technical maturity [62,63]. However, they are limited by their low removal efficiency in anodic oxidation. The Pt electrode was used to degrade organic pollutants including organic chemical raw materials (e.g., phenol) and medicine (e.g., sulfadiazine) due to its good electrical conductivity and durability when treating wastewater [64,65], but its industrial mass production and application are limited by its price (920 $ per ounce). Similarly, the BDD electrode has excellent degradation and recyclability of organic pollutants [54], but its use is limited due to its high cost of about 984 $ per 8 cm^2 [66]. The Ru-SnO_2 and PbO_2 electrodes are often applied to pollutant degradation process due to their high technical maturity, low cost and corrosion resistance [63,67]. But the removal efficiency of organic pollutants is low in the electrolysis process with the Ru-SnO_2 and PbO_2 electrodes [63]. By comparison, the ANT removal efficiency in 0.1 M Na_2SO_4 solutions was 91.28% with the Mn-PbO_2 electrode (k=0.021 min^{-1}). In addition, Mn (2,324 $ per ton) has a lower price relative to other rare metals (e.g., Ru, 480 $ per ounce) and the

Table 1. The comparison of different electrodes

Anode	Cathode	Pollutants	Conditions	Results	Cost /8 cm^2	Ref.
PbO_2	Ti	1 mg/L ANT	Na_2SO_4: 0.1 M 20 mA/cm^2 Surface area (SA): 8 cm^2	k_{obs}: 0.0041 min^{-1}	3.52 $	This study
Mn-PbO_2	Ti	1 mg/L ANT	Na_2SO_4: 0.1 M 20 mA/cm^2 SA: 8 cm^2	k_{obs}: 0.0206 min^{-1}	3.53 $	
BDD	Carbon felt	1 mg/L ANT	$NaNO_3$: 0.05 M 10 mA/cm^2 SA: 8 cm^2	k_{obs}: 0.0232 min^{-1}	984 $	[54]
Ru-IrO_2	Pt plaque	100 mg/L methylene blue (MB)	NaCl: 0.03 M 40 mA/cm^2 SA: 1 cm^2	50% MB removal: 70-80 min	-	[62]
Ru-SnO_2	Cu/Zn alloy	50 mg/L Aniline	Na_2SO_4: 0.05 M 20 mA/cm^2 SA: 64.5 cm^2, pH 3	50% Aniline removal: 90 min	-	[63]
Ru-IrO_2				50% Aniline removal: 270 min	-	
Pt	-	0.02 mM Sulfadiazine Sulfamerazine	Na_2SO_4: 0.05 M 20 mA/cm^2 pH 7	k_{obs}: 0.0026-0.0028 min^{-1}	-	[64]
Pt	Ti	490 mg/L Phenol	Na_2SO_4: 0.25 M 20 mA/cm^2 SA: 6 cm^2, pH 6	50% Phenol removal: 5 h 50% TOC: removal: 35 h	-	[65]

Note: The cost of anode (8 cm^2) was estimated based on the market price.

preparation cost of PbO_2 electrode was not significantly increased by doping Mn into PbO_2 electrode (only 3.53 $ per 8 cm^2). Therefore, the Mn-PbO_2 electrode has certain potential in removing pollutants because of its low cost and good removal efficiency.

CONCLUSION

Mn-PbO_2 electrodes with excellent electrocatalytic activity were prepared via a combination of sol-gel and electrodeposition methods. The Mn-PbO_2 electrode exhibited a larger electrochemically active surface area than the PbO_2 electrode. When the Mn-PbO_2 electrode was used as the anode, the ANT degradation efficiency reached 91.28% after 120 min electrolysis in 0.1 M Na_2SO_4 solution containing 1 mg/L ANT at a constant current density of 20 mA/cm^2 and an initial pH of 7. Moreover, MnO_4^- with strong oxidizability was generated in the Na_2SO_4 solution, which is beneficial to improving the degradation efficiency, and the combination of MnO_4^- and the DET process played a major role in improving the ANT removal efficiency rather than ROS, which is considered to play an important role in the oxidation of pollutants. In addition, the Mn-PbO_2 electrode achieved a good effect after the 1st and 10th degradation cycles, and there was no secondary pollution of metals in the electrolysis process. Overall, the Mn-PbO_2 electrode has practical application prospects for organic pollutant degradation, given the remarkable degradation efficiency and the remarkable removal efficiency in the wide pH range.

ACKNOWLEDGEMENT

This work was supported by the National Natural Science Foundation of China (Grant No. 42177032) and the National Key R&D Program of China (Grant No. 2018YFC1802005). We thank LetPub for its linguistic assistance during the preparation of this manuscript.

STATEMENTS & DECLARATIONS

Ethical Approval

Not applicable.

Consent to Participate

All authors read and approved the final manuscript.

Consent to Publish

The institute (Institute of Soil Science, Chinese Academy of Sciences) and the university (University of Chinese Academy of Sciences) all agreed to publish this manuscript in *Korean Journal of Chemical Engineering*.

Author Contributions

Jingjin Zhou: Methodology, Data curation, Writing-original draft preparation

Xiuzhen Hao: Data curation, Writing-reviewing and editing

Longgang Chu: Methodology
Long Cang: Writing-reviewing and editing

Funding

This work was supported by the National Natural Science Foundation of China (Grant No. 42177032) and the National Key R&D Program of China (Grant No. 2018YFC1802005).

Competing Interests

The authors have no relevant financial or non-financial interests to disclose.

Availability of Data and Materials

Not applicable.

SUPPORTING INFORMATION

Additional information as noted in the text. This information is available via the Internet at http://www.springer.com/chemistry/journal/11814.

REFERENCES

1. X. Du, M. A. Oturan, M. Zhou, N. Belkessa, P. Su, J. Cai, C. Trellu and E. Mousset, *Appl. Catal. B-Environ.*, **296**, 120332 (2021).
2. R. V. McQuillan, G. W. Stevens and K. A. Mumford, *J. Hazard. Mater.*, **383**, 121244 (2020).
3. S. W. da Silva, E. M. O. Navarro, M. A. S. Rodrigues, A. M. Bernardes and V. Perez-Herranz, *J. Electroanal. Chem.*, **832**, 112 (2019).
4. F. Sopaj, M. A. Rodrigo, N. Oturan, F. I. Podvorica, J. Pinson and M. A. Oturan, *Chem. Eng. J.*, **262**, 286 (2015).
5. H. Lin, J. Niu, S. Ding and L. Zhang, *Water Res.*, **46**, 2281 (2012).
6. L. A. Perea, R. E. Palma-Goyes, J. Vazquez-Arenas, I. Romero-Ibarra, C. Ostos and R. A. Torres-Palma, *Sci. Total Environ.*, **648**, 377 (2019).
7. L. Labiadh, A. Barbucci, M. P. Carpanese, A. Gadri, S. Ammar and M. Panizza, *J. Electroanal. Chem.*, **766**, 94 (2016).
8. R. Xie, X. Meng, P. Sun, J. Niu, W. Jiang, L. Bottomley, D. Li, Y. Chen and J. Crittenden, *Appl. Catal. B-Environ.*, **203**, 515 (2017).
9. N. Gedam, N. R. Neti, M. Kormunda, J. Subrt and S. Bakardjieva, *Electrochim. Acta*, **169**, 109 (2015).
10. S. Alcocer, A. Picos, A. R. Uribe, T. Perez and J. M. Peralta-Hernandez, *Chemosphere*, **205**, 682 (2018).
11. Y. Jiang, Z. Hu, M. Zhou, L. Zhou and B. Xi, *Sep. Purif. Technol.*, **128**, 67 (2014).
12. Y. Liu and H. Liu, *Electrochim. Acta*, **53**, 5077 (2008).
13. G. Bonyadinejad, M. Sarafraz, M. Khosravi, A. Ebrahimi, S. M. Taghavi-Shahri, R. Nateghi and S. Rastaghi. *Korean J. Chem. Eng.*, **33**(1), 189 (2016).
14. S. Song, J. Fan, Z. He, L. Zhan, Z. Liu, J. Chen and X. Xu, *Electrochim. Acta*, **55**, 3606 (2010).
15. Y. Xia, J. Feng, S. Fan, W. Zhou and Q. Dai, *Chemosphere*, **263**, 128069 (2021).
16. J. Hu, X. Bian, Y. Xia, M. Weng, W. Zhou and Q. Dai, *Sep. Purif. Technol.*, **250**, 117109 (2020).
17. Y. Yao, M. Li, Y. Yang, L. Cui and L. Guo, *Chemosphere*, **216**, 812 (2019).
18. M. Xu, Z. Wang, F. Wang, P. Hong, C. Wang, X. Ouyang, C. Zhu, Y. Wei, Y. Hun and W. Fang, *Electrochim. Acta*, **201**, 240 (2016).
19. P. Li, Y. Zhao, B. Ding and L. Wang, *J. Electroanal. Chem.*, **747**, 45 (2015).
20. Z. Lv, Z. Chen, Q. Yu, W. Zhu, H. You, B. Chen, Z. Zheng, Y. Liu and Q. Hu, *RSC Adv.*, **11**, 28949 (2021).
21. Y. G. Gu, H. B. Li and H. B. Lu, *Ecol. Eng.*, **101**, 179 (2017).
22. R. Chen, J. Lv, W. Zhang, S. Liu and J. Feng, *Environ. Earth. Sci.*, **74**, 2743 (2015).
23. A. Desaules, S. Ammann, F. Blum, R. C. Brandli, T. D. Bucheli and A. Keller, *J. Environ. Monitor.*, **10**, 1265 (2008).
24. T. Cai, Y. Ding, Z. Zhang, X. Wang, T. Wang, Y. Ren and Y. Dong, *Environ. Pollut.*, **254**, 112981 (2019).
25. R. Lopez-Vizcaino, J. Alonso, P. Canizares, M. J. Leon, V. Navarro, M. A. Rodrigo and C. Saez, *J. Hazard. Mater.*, **265**, 142 (2014).
26. H. Lin, J. Niu, J. Xu, Y. Li and Y. Pan, *Electrochim. Acta*, **97**, 167 (2013).
27. X. Tan, Y. Zhao, W. Sun, C. Jin, L. Chen, H. Wei and C. Sun, *J. Electroanal. Chem.*, **856**, 113726 (2020).
28. B. Tang, L. Zhang and Y. Geng, *Talanta*, **65**, 769 (2005).
29. L. Chen, X. Peng, J. Liu, J. Li and F. Wu, *Ind. Eng. Chem. Res.*, **51**, 13632 (2012).
30. Y. Xia, X. Bian, Y. Xia, W. Zhou, L. Wang, S. Fan, P. Xiong, T. Zhan, Q. Dai and J. Chen, *Sep. Purif. Technol.*, **237**, 116321 (2020).
31. D. Devilliers, M. T. D. Thi, E. Mahe and Q. L. Xuan, *Electrochim. Acta*, **48**, 4301 (2003).
32. B. Zhao, H. Yu, Y. Lu, J. Qu, S. Zhu and M. Huo, *J. Taiwan Inst. Chem. Eng. E.*, **100**, 144 (2019).
33. H. T. Yang, B. M. Chen, Z. C. Guo, H. R. Liu, Y. C. Zhang, H. Huang, R. D. Xu and R. C. Fu, *T. Nonferr. Metal. Soc.*, **24**, 3394 (2014).
34. Y. Wang, M. Chen, C. Wang, X. Meng, W. Zhang, Z. Chen and J. Crittenden, *Chem. Eng. J.*, **374**, 626 (2019).
35. P. Duan, S. Gao, J. Lei, X. Li and X. Hu, *Environ. Pollut.*, **263**, 114436 (2020).
36. M. C. Biesinger, B. P. Payne, A. P. Grosvenor, L. W. M. Lau, A. R. Gerson and R. S. C. Smart, *Appl. Surf. Sci.*, **257**, 2717 (2011).
37. M. Xu, Y. Mao, W. Song, X. OuYang, Y. Hu, Y. Wei, C. Zhu, W. Fang, B. Shao, R. Lu and F. Wang, *J. Electroanal. Chem.*, **823**, 193 (2018).
38. P. J. Blood, I. J. Brown and S. Sotiropoulos, *J. Appl. Electrochem.*, **34**, 1 (2004).
39. H. Mo, Y. Tang, N. Wang, M. Zhang, H. Cheng, Y. Chen, P. Wan, Y. Sun, S. Liu and L. Wang, *J. Solid State Electr.*, **20**, 2179 (2016).
40. X. Zhou, S. Liu, A. Xu, K. Wei, W. Han, J. Li, X. Sun, J. Shen, X. Liu and L. Wang, *Chem. Eng. J.*, **330**, 956 (2017).
41. L. Yu, J. Xue, L. Zhang, C. Tang and Y. Guo, *Electrochim. Acta*, **368**, 137532 (2021).
42. L. Chen, C. Lei, Z. Li, B. Yang, X. Zhang and L. Lei, *Chemosphere*, **210**, 516 (2018).
43. H. Yu, Y. Song, B. Zhao, Y. Lu, S. Zhu, J. Qu, X. Wang and W. Qin, *Electrocatalysis*, **9**, 725 (2018).
44. W. Zhao, J. Xing, D. Chen, D. Jin and J. Shen, *J. Electroanal. Chem.*, **775**, 179 (2016).
45. C. Salazar, N. Contreras, H. D. Mansilla, J. Yanez and R. Salazar, *J. Hazard. Mater.*, **319**, 84 (2016).
46. H. Xu, Q. Yuan, D. Shao, H. Yang, J. Liang, J. Feng and W. Yan, *J.*

Hazard. Mater., **286**, 509 (2015).
47. F. Wei, D. Liao, Y. Lin, C. Hu, J. Ju, Y. Chen and D. Feng, *Sep. Purif. Technol.*, **258**, 118056 (2021).
48. S. Chen, P. He, X. Wang, F. Xiao, P. Zhou, Q. He, L. Jia, F. Dong, H. Zhang, B. Jia, H. Liu and B. Tang, *Chemosphere*, **268**, 128799 (2021).
49. S. Chen, J. Li, L. Liu, Q. He, L. Zhou, T. Yang, X. Wang, P. He, H. Zhang and B. Jia, *Chemosphere*, **256**, 127129 (2020).
50. P. Maharaja, R. Boopathy, S. Karthikeyan, M. Mahesh, A. S. Komal, V. K. Gupta and G. Sekaran, *J. Environ. Sci. Technol.*, **13**, 2143 (2016).
51. A. Mirza, M. Burr, T. Ellis, D. Evans, D. Kakengela, L. Webb, J. Gagnon, F. Leclercq and A. Johnston, *J. S. Afr. I. Min Metall.*, **116**(6), 533 (2016).
52. J. Iniesta, J. Gonzalez-Garcia, E. Exposito, V. Montiel and A. Aldaz, *Water Res.*, **35**(14), 3291 (2001).
53. D. Wang, Y. Li, M. Yang and M. Han, *Sci. Total Environ.*, **393**, 64 (2008).
54. L. Chu, Z. Sun, L. Cang, G. Fang, X. Wang, D. Zhou and J. Gao, *Chem. Eng. J.*, **400**, 125945 (2020).
55. A. Mallakin, B. J. McConkey, G. B. Miao, B. McKibben, V. Snieckus, D. G. Dixon and B. M. Greenberg, *Ecotox. Environ. Safe.*, **43**, 204 (1999).
56. C. Liang, Z. S. Wang and C. J. Bruell, *Chemosphere*, **66**, 106 (2007).
57. G. D. Fang, D. M. Zhou and D. D. Dionysiou, *J. Hazard. Mater.*, **250-251**, 68 (2013).
58. X. Duan, C. Zhao, W. Liu, X. Zhao and L. Chang, *Electrochim. Acta*, **240**, 424 (2017).
59. T. Xu, Z. Wang, Y. Ding, W. Xu, W. Wu, Z. Zhu and H. Fong, *Carbohyd. Polym.*, **179**, 164 (2018).
60. S. W. da Silva, E. M. O. Navarro, M. A. S. Rodrigues, A. M. Bernardes and V. Perez-Herranz, *Chemosphere*, **210**, 615 (2018).
61. S. Garcia-Segura, E. V. dos Santos and C. A. Martinez-Huitle, *Electrochem. Commun.*, **59**, 52 (2015).
62. A. Baddouh, B. El Ibrahimi, M. M. Rguitti, E. Mohamed, S. Hussain and L. Bazzi, *Sep. Sci. Technol.*, **55**, 1852 (2019).
63. X. Zhu, W. Hu, C. Feng, N. Chen, H. Chen, P. Kuang, Y. Deng and L. Ma, *Chemosphere*, **269**, 128734 (2021).
64. H. Li, H. Jiang, C. Liu, C. Zhu and X. P. Zhu, *ChemistryOpen*, **8**, 1421 (2019).
65. X. Y. Li, Y. H. Cui, Y. J. Feng, Z. M. Xie and J. D. Gu, *Water Res.*, **39**, 1972 (2005).
66. A. Dirany, I. Sires, N. Oturan, A. Ozcan and M. A. Oturan, *Environ. Sci. Technol.*, **46**, 4074 (2012).
67. Y. H. Cui, X. Y. Li and G. Chen, *Water Res.*, **43**, 1968 (2009).

Supporting Information

Effect of manganese doping on the PbO_2 electrode for the enhanced electrochemical oxidation of anthracene: Optimization and mechanism

Jinjin Zhou[*,], Xiuzhen Hao[*], Longgang Chu[*,**], and Long Cang[*,†]**

*Key Laboratory of Soil Environment and Pollution Remediation, Institute of Soil Science, Chinese Academy of Sciences, Nanjing 210008, China
**University of Chinese Academy of Sciences, Beijing 100049, China
(*Received 11 July 2022 • Revised 24 November 2022 • Accepted 16 December 2022*)

Text S1. Procedure of GC-MS to analyze intermediates.

The intermediates of ANT were analyzed with GC-MS in the following steps: firstly, adding 3 mL extracting agent (1 : 1 v/v dichloromethane to n-hexane) was into 10 mL withdrawn sample solution and mixed well; then, the mixed solution was kept shaking for 4 h and allowed to set still for 1 h; finally, 1 mL of the supernatant was taken and added into a GC vial, in which sodium sulfate was pre-added, and stored in refrigerator till analysis.

Text S2. Procedure of solid phase extraction (SPE) to analyze intermediates.

Before analyzing intermediates of ANT by LC-TOF-MS, samples during oxidation were extracted and desalinated by the SPE method with Poly-Sery HLB cartridge (ANPEL, Shanghai) in the following steps: firstly, the cartridge was treated with 5 mL methanol and 5 mL ultrapure water both for 3 times; then, 50 mL sample was added into the cartridge; then, 5 mL ultrapure water was added into the cartridge for cleaning; finally, 1 mL methanol was added into the cartridge to extract products, and the eluted solution was collected and stored in the refrigerator till analysis.

Text S3. Instrumental parameters of EPR.

The instrumental parameters of EPR were as follows: a center field of 3,480 G, resonance frequency of 9.837 GHz, sweep width of 50 G, microwave power of 6.33 mW and modulation frequency of 100 kHz. The concentration of DMPO was about 100 mM.

Text S4. Procedure of analyzing the $^{\bullet}OH$ concentration.

To analyze $^{\bullet}OH$ formation from the anode (PbO_2 electrode or Mn-PbO_2 (3 mM) electrode), no ANT was added in the system in stead of 0.5 mM TPA, and electrolyte solution was 0.1 M Na_2SO_4 solution and the constant current density was 20 mA/cm^2. Electrolyte solution pH was adjusted to 6.5-7.0 by NaOH to dissolve TPA. The $^{\bullet}OH$ radicals react with TPA to generate 2-hydroxy terephthalic acid (hTPA) during electrocatalytic oxidation, which has a fluorescence signal at about 425 nm and determined by RF-20A (Shimazu, Japan). The concentration of $^{\bullet}OH$ was be estimated from the concentration of hTPA divided by 0.35.

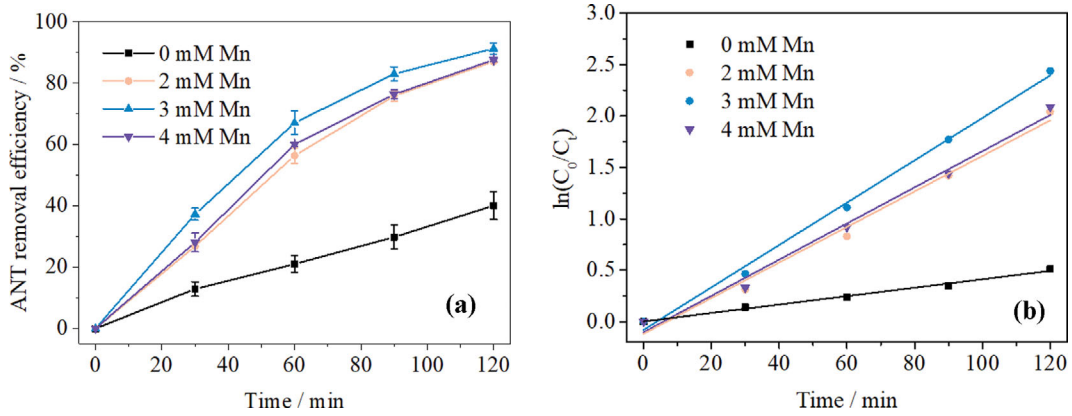

Fig. S1. The effect of $Mn(NO_3)_2$ concentration in electroplating solution on (a) the ANT removal efficiency and (b) the corresponding kinetics analysis in 0.1 M Na_2SO_4 solution (current density: 20 mA/cm^2; initial pH: 7±0.3; initial ANT concentration: 1 mg/L).

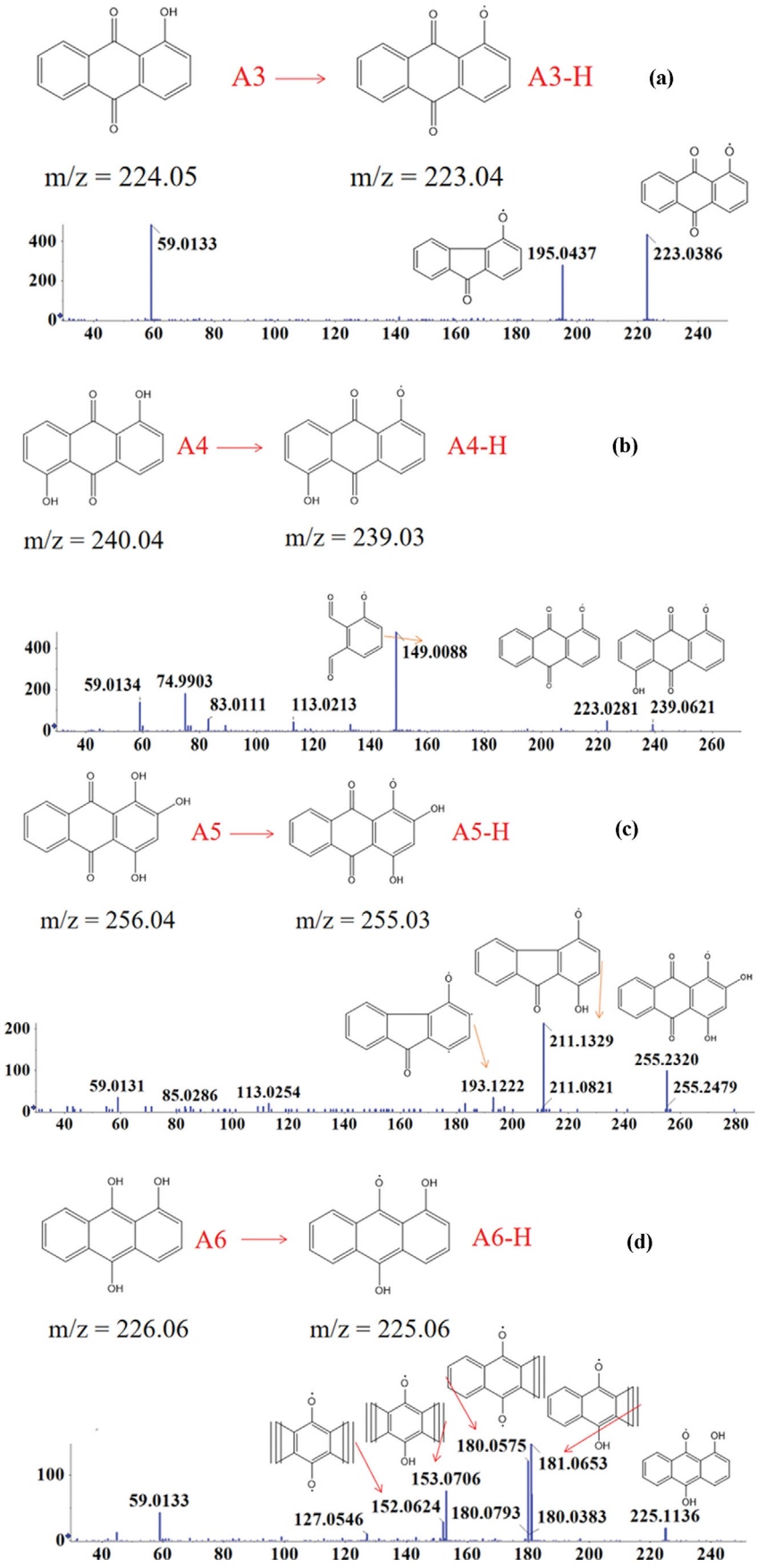

Fig. S2. MS/MS spectra of ANT intermediates of ANT in LC-TOF-MS: (a) 1-hATQ, (b) 1,5-dhATQ, (c) 1,2,4-thATQ, (d) 1,9,10-thANT.

Table S1. Intermediates of ANT identified by GC-MS and LC-TOF-MS

Number	m/z	Name	Detection method	Structural formula
A1	198	ANT	GC-MS	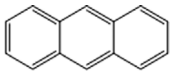 ($C_{14}H_{10}$)
A2	208	Anthraquinone (ATQ)	GC-MS	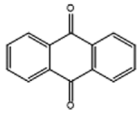 ($C_{14}H_8O_2$)
A3	$[M-H]^-$: 223	1-Hydroxy ATQ	LC-TOF-MS	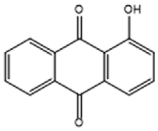 ($C_{14}H_8O_3$)
A4	$[M-H]^-$: 239	1,5-Dihydroxy ATQ	LC-TOF-MS	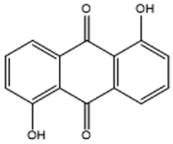 ($C_{14}H_8O_4$)
A5	$[M-H]^-$: 255	1,2,4-Trihydroxy ATQ	LC-TOF-MS	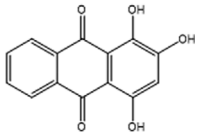 ($C_{14}H_{10}O_3$)
A6	$[M-H]^-$: 225	1,9,10-Trihydroxy ANT	LC-TOF-MS	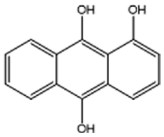 ($C_{14}H_{10}O_3$)

Table S2. The concentration of leaching metals in 0.1 mol/L Na_2SO_4 solution (20 mA/cm^2)

Electrodes	Concentration (mg/L)	0 min	30 min	60 min	90 min	120 min
PbO_2	Pb	ND	ND	ND	ND	ND
Mn-PbO_2		ND	ND	ND	ND	ND
PbO_2	Sb	ND	ND	ND	ND	ND
Mn-PbO_2		ND	ND	ND	ND	ND

Note: the detection limit was 0.1 mg/L for Pb and Sb.

Table S3. Predicted acute toxicity of ANT and transformation products based on ECOSAR

Products	Structure	Type of intermediates	Acute toxicity (mg/L)		
			Fish	daphnia	Green algae
			LC50	LC50	EC50
A1	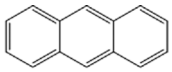	Neutral Organics	1.147	0.809	1.475
A2	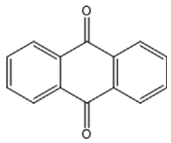	Neutral Organics	10.610	6.821	8.488
A3	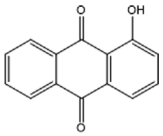	Phenols	2.203	1.378	5.402
A4	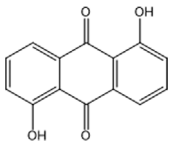	Phenols, Poly	0.901	3.270	1.113
A5	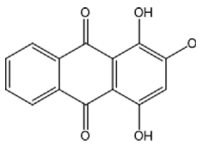	Phenols, Poly	1.858	8.156	1.726
A6	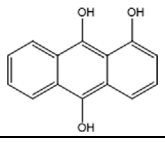	Phenols, Poly	3.504	19.169	2.344